High-Threshold Codes for Neutral-Atom Qubits with Biased Erasure Errors

Kaavya Sahay,[1,2,*] Junlan Jin,[3,*] Jahan Claes,[1,2] Jeff D. Thompson,[3] and Shruti Puri[1,2]

[1]*Yale University, Department of Applied Physics, New Haven, Connecticut 06520, USA*
[2]*Yale Quantum Institute, Yale University, New Haven, Connecticut 06511, USA*
[3]*Princeton University, Department of Electrical and Computer Engineering, Princeton, New Jersey 08544, USA*

(Received 4 April 2023; revised 10 July 2023; accepted 6 September 2023; published 24 October 2023)

The requirements for fault-tolerant quantum error correction can be simplified by leveraging structure in the noise of the underlying hardware. In this work, we identify a new type of structured noise motivated by neutral-atom qubits, biased erasure errors, which arises when qubit errors are dominated by detectable leakage from only one of the computational states of the qubit. We study the performance of this model using gate-level simulations of the *XZZX* surface code. Using the predicted erasure fraction and bias of metastable ^{171}Yb qubits, we find a threshold of 8.2% for two-qubit gate errors, which is 1.9 times higher than the threshold for unbiased erasures and 7.5 times higher than the threshold for depolarizing errors. Surprisingly, the improved threshold is achieved without bias-preserving CONTROLLED-NOT gates and, instead, results from the lower noise entropy in this model. We also introduce an *XZZX* cluster state construction for measurement-based error correction, hybrid fusion, that is optimized for this noise model. By combining fusion operations and deterministic entangling gates, this construction preserves the intrinsic symmetry of the *XZZX* code, leading to a higher threshold of 10.3% and enabling the use of rectangular codes with fewer qubits. We discuss a potential physical implementation using a single plane of atoms and movable tweezers.

DOI: 10.1103/PhysRevX.13.041013 Subject Areas: Quantum Information

I. INTRODUCTION

Quantum error correction (QEC) is essential to protect fragile quantum states during computation [1–3]. To achieve scalable quantum computation, the rate at which errors are introduced must be below a threshold error rate that depends on the noise model and error correction approach [4–7]. Recently, significant work has focused on identifying or engineering the structure of noise in qubits, which can lead to higher thresholds and reduced overhead if paired with appropriate gate operations and QEC architectures. For example, biased Pauli noise models can be engineered in superconducting cat qubits [8–10] and certain neutral-atom qubits [11]. Given the availability of bias-preserving gates [12], this can lead to significantly improved thresholds and lower overhead for the *XZZX* surface code, which has special symmetries facilitating decoding this type of noise [13,14]. Another example is qubits where errors can be converted with high probability into erasure errors. This model has been proposed for appropriately engineered qubit encodings and gates in neutral atoms [15], trapped ions [16], and superconducting qubits [17,18] and leads to significantly increased thresholds [15–17,19–21].

In this work, we identify a new structured error, *biased erasure error*, that arises when noise is dominated by erasures from only one computational state of the qubit. This model is physically motivated by metastable ^{171}Yb qubits, where erasures result from leakage out of the $|1\rangle$ computational state into levels whose population can be continuously monitored using cycling transitions that do not affect the qubit levels [15,22]. We refer to this as a (Z-) biased erasure model, as detecting transitions outside the computational states reveals that the qubit was previously in $|1\rangle$, and can be represented as a Z error with 50% probability. The biased erasure model has more structure than the conventional erasure model, where observing an erasure yields no information about the prior state of the qubit [15–17,19–21,23]. Indeed, the error rate at which the quantum capacity of such a channel becomes positive is twice that of the conventional erasure channel, indicating that error correction threshold for the biased erasure channel can be much higher than that of the conventional erasure channel [24].

In this work, we study the performance of error correction against biased erasures at the circuit level in several

[*]These authors contributed equally to this work.

TABLE I. Summary of thresholds derived in this work for the $XZZX$ surface code under various error models and QEC architectures. Thresholds are obtained using an MWPM decoder and are reported for several values of R_e. The first three rows give thresholds using circuit-based syndrome extraction (Sec. III), for unbiased erasures [15], and using the biased erasure model in Sec. II. The latter error model is studied with and without bias-preserving CX gates, where the former case corresponds to the native gates (single-qubit gates and CZ) of the neutral-atom platform. The last line is the hybrid-fusion error correction scheme introduced in Sec. IV, with native gates. The final two columns indicate additional properties discussed in detail in Sec. V: whether the dominant errors produce pairs of syndromes lying in 2D planes of the decoding graph (reducing qubit overhead in the limit of large bias) and whether midcircuit atom replacement is necessary to recover from erasure errors. The dagger indicates that this numerically simulated threshold increases to 17.7% when using an erasure decoder at large system sizes (see the text).

Model	$R_e = 0$	$R_e = 0.98$	$R_e = 1$	Preserves 2D symmetry?	Avoids atom replacement?
Circuit, unbiased erasures	1.1%	4.3%	5.0%	N	N
Circuit, biased erasures, native gates	1.1%	8.2%	10.3%	N	N
Circuit, biased erasures, BCX	1.1%	9.0%	12.8%	Y	N
Hybrid-fusion, native gates	1.0%	10.3%	14.7%†	Y	Y

contexts. We first consider the $XZZX$ surface code with conventional, circuit-based syndrome extraction. We find a threshold of 8.2% when biased erasures comprise $R_e = 0.98$ of the two-qubit gate errors, as predicted for ^{171}Yb under optimal conditions [15]. This is nearly double the threshold of 4.3% for a conventional erasure model and approximately 8 times the threshold in a comparable depolarizing error model. The high threshold, compared to depolarizing noise, highlights the benefit of engineering qubits with this favorable error model. Remarkably, this high threshold is obtained using only the native gate set of neutral-atom qubits: single-qubit gates and controlled-Z (CZ) gates, without bias-preserving controlled-NOT (CX) gates. We attribute the higher threshold to a lower noise entropy when erasures are biased compared to when they are not.

We also introduce a measurement-based QEC architecture, *hybrid fusion*, that is specifically tailored for neutral-atom qubits with biased erasure noise. This approach combines fusion operations with deterministic entangling gates to construct an $XZZX$ cluster state while preserving the symmetry of the $XZZX$ code under biased noise, without requiring bias-preserving CX gates. In fusion-based error correction, an error-correcting code is built by fusing together few-body entangled resource states using measurements of two-qubit Pauli operators $X \otimes X$ and $Z \otimes Z$. This method has been studied in linear optical quantum computing, where nondeterministic heralded fusions are the native entangling operation [25–29], and has the benefit of preserving the symmetry of the $XZZX$ code when the fusion errors are biased [29]. We present a bias-preserving fusion circuit for qubits with biased erasures and combine this operation with deterministic entangling gates to develop a measurement-based error correction architecture with a high threshold and reduced overhead. With this approach, we find an even higher threshold of 10.3% for $R_e = 0.98$. We also discuss other potential advantages of this approach for neutral atoms including robustness against atom loss and relaxed requirements for erasure detection and atom replacement.

This noise model is physically motivated by metastable ^{171}Yb qubits [15]. Recent experimental work has demonstrated high-fidelity gates and validated the basic concept of erasure conversion in this platform, by performing midcircuit detection of erasure errors with a strong bias from one of the two qubit levels [30]. Erasure-dominated error models may also be engineered in other qubits with prevalent erasure errors such as metastable trapped-ion qubits [16], superconducting qubits encoded in the $|g\rangle$, $|f\rangle$ levels of transmons [17], or dual-rail superconducting qubits [18] (see Refs. [31,32] for recent experimental demonstrations). The high thresholds and reduced requirements for bias-preserving gate operations may encourage the development of new qubits or encodings. Finally, this work may stimulate further development of fusion-based QEC architectures for neutral atoms.

The main results of our work are summarized in Table I. We introduce the biased erasure error model in Sec. II and study its behavior using circuit-based error correction in Sec. III. In Sec. IV, we introduce the hybrid-fusion architecture and study its performance. We discuss further opportunities for optimization in Sec. V and conclude in Sec. VI.

II. BIASED ERASURE ERRORS IN NEUTRAL ATOMS

To motivate the biased erasure model, we consider how it arises naturally in neutral-atom qubits. In this platform, the dominant source of errors are two-qubit gates implemented using the Rydberg blockade [33–36] (single-qubit and idling errors are comparatively much lower [30]). The only fundamental effect limiting the fidelity of two-qubit gates is the finite lifetime of the Rydberg state that is populated transiently during the gate [37]. In the particular case of ^{171}Yb [35,38], encoding the qubit in the nuclear spin sublevels of the metastable $^3P_0$ level has the property that the majority of the decay events populate disjoint subspaces whose occupation can be detected efficiently,

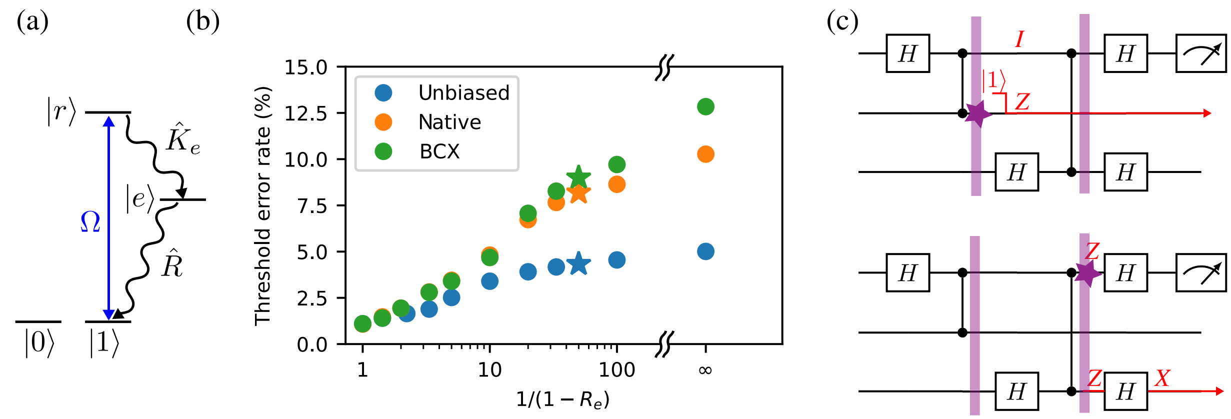

FIG. 1. (a) Biased erasures arise when erasures (leakage to a detectable state $|e\rangle$) occur from only one qubit state, $|1\rangle$, such that recovery by replacement or reinitialization in the same state results in at most a Z error. (b) Threshold error rates as a function of R_e, under different error models: unbiased erasures (blue), biased erasures with native gates (orange), and biased erasures with bias-preserving CX (BCX) gates (green). The stars denote $R_e = 0.98$. (c) Illustrative circuit measuring the two-qubit stabilizer ZX using native gates. When an erasure is detected during a two-qubit gate (purple star, depicting fluorescence detection of an atom in $|e\rangle$), the affected atom is replaced in $|1\rangle$ and the resulting state is described by an error drawn from $\{I, Z\}^{\otimes 2}$, but the manner in which this error propagates depends on its space-time location in the circuit. If the error occurs during the Z measurement (top), it propagates to the end of the circuit as a Z error. If the error occurs during the X measurement (bottom), it propagates to the end of the circuit as an X error. Knowledge of the error location makes this information available to the decoder, lowering the entropy of the noise.

which converts these errors into erasure errors [15,22]. Recent additional work has derived gate protocols to convert other errors such as quasistatic laser noise and Doppler shifts into erasure errors through a similar mechanism [39,40].

In this work, we consider an additional property of the physical error model of metastable ^{171}Yb qubits, which is that excitation to the Rydberg state $|r\rangle$ occurs only from the qubit state $|1\rangle$ and never from $|0\rangle$ [Fig. 1(a)] [11]. To illustrate the behavior of this model, consider a hypothetical single-qubit operation involving excitation from $|1\rangle$ to $|r\rangle$, where the only possible error is a decay from $|r\rangle$ to a detectable, disjoint state $|e\rangle$. In the absence of an error, the qubit is coherently deexcited back to $|1\rangle$ at the end of the gate. This results in a quantum channel with Kraus operators:

$$K_0 = |0\rangle\langle 0| + \sqrt{1-2p_e}|1\rangle\langle 1| + |e\rangle\langle e|, \tag{1}$$

$$K_e = \sqrt{2p_e}|e\rangle\langle 1|. \tag{2}$$

The probability of an error, averaged over both computational states, is p_e.

Upon detection of an atom in $|e\rangle$, the qubit is reinitialized into $|1\rangle$ or replaced by a new qubit in $|1\rangle$, described by the recovery operator $\hat{R} = |1\rangle\langle e|$. The combined channel can be expressed by the Kraus operators:

$$W_0 = |0\rangle\langle 0| + \sqrt{1-2p_e}|1\rangle\langle 1|, \tag{3}$$

$$W_e = \hat{R}K_e = \sqrt{2p_e}|1\rangle\langle 1|. \tag{4}$$

We obtain an effective Pauli channel using the identity $|1\rangle\langle 1| = (I-Z)/2$ and the Pauli twirl approximation (PTA), which may be achieved in practice by inserting random single-qubit Pauli gates after atom replacement [41–43]. The portion of the channel describing the erasure error is

$$W_e \rho W_e^\dagger = \frac{p_e}{2}(I\rho I + Z\rho Z). \tag{5}$$

Since the resulting state has at most a Z error, we refer to this as a *biased erasure* error model.

To model a two-qubit CZ gate, we incorporate two additional considerations. First, the leakage of one atom can result in a dephasing error on the other atom as well [44]. Therefore, a two-qubit gate with an average erasure probability p_e is modeled by drawing an operator from the set $\{I, Z\}^{\otimes 2}$ with uniform probability $p_e/4$. Second, there is also a finite rate of nonerasure errors such as decays from $|r\rangle$ back to the qubit subspace. We model these as depolarizing errors with total rate p_p by drawing an operator from the set $\{I, X, Y, Z\}^{\otimes 2} \backslash \{I \otimes I\}$ with uniform probability $p_p/15$. The relative probability of these errors is given by the branching ratio $R = p_e/(p_e + p_p)$, which depends on the underlying physics of the qubit. For metastable ^{171}Yb, we predict $R = 0.98$ [15].

In this work, we consider only errors during two-qubit gates, which are by far the dominant errors for neutral atoms. A discussion of the role of measurement, single-qubit gate, and idling errors on the unbiased erasure model can be found in Ref. [15].

Lastly, we note that the no-jump error also contributes a Z-biased Pauli error with probability Ap_e^2 because of the asymmetry in the erasure probability from the two qubit states [11,15]. Continuing the previous example of a single-qubit gate, the evolution under the Kraus operator from Eq. (3) is

$$W_0 \rho W_0^\dagger \approx \left(1 - p_e - \frac{p_e^2}{4}\right) I \rho I + \frac{p_e^2}{4} Z \rho Z. \tag{6}$$

Here, we apply the PTA and take the limit $p_e \ll 1$.

We find a Pauli error rate of Ap_e^2 with $A = 1/4$ in Eq. (6), but for the two-qubit gate we estimate $A \approx 1/12$ [44]. We incorporate this by increasing the Pauli error probability to $p_p' = p_p + Ap_e^2$. In the resulting model, erasures constitute a fraction R_e of all errors, with R_e given by

$$R_e = \frac{p_e}{p_p' + p_e} = \frac{R}{1 + AR^2(p_p + p_e)}. \tag{7}$$

To present a more generalizable model of biased erasures, we consider the error model to be defined by the independent parameters R_e and $p = p_p' + p_e$. Far below the threshold ($p \ll 1$), the behavior of ^{171}Yb can be estimated by setting $R_e = R = 0.98$. However, the performance near the threshold is slightly different, since $R_e < R$. We note that $R_e = 1$ is not physically attainable for any value of R but may be achievable in other physical models of biased erasure if both computational states leak with equal rates but to disjoint final states such that the Z information is preserved.

III. CIRCUIT-BASED QEC WITH BIASED ERASURES

We quantify the advantage of the biased erasure model using circuit-level simulations of the $XZZX$ code. The simulations use square codes with distance d up to 13, implemented as d rounds of noisy stabilizer measurements followed by a final, noiseless stabilizer measurement [44]. The error syndromes are decoded using a minimum-weight perfect matching (MWPM) decoder, adjusting edge weights in each shot to incorporate the location of the erasure errors. The stabilizer simulations and construction of the decoding graph are implemented with STIM [45], while the decoding is implemented with PyMatching [46]. Except where noted, the simulations do not consider bias-preserving CX gates. Therefore, CX gates are implemented using CZ gates, conjugated by Hadamard (H) gates, which convert Z errors on the target qubit into X errors.

In Fig. 1(b), we show the threshold error rate p_{th} as a function of R_e. For comparison, we show three cases: unbiased erasures, biased erasures using only the native gates of the Rydberg platform, and biased erasures incorporating hypothetical bias-preserving CX gates.

For large values of R_e, biased erasures result in significantly higher thresholds than unbiased erasures, even in the absence of bias-preserving gates. For example, at the value $R_e = 0.98$ projected for metastable ^{171}Yb qubits, the threshold is 8.2%, nearly twice the value with unbiased erasures ($p_{\text{th}} = 4.3\%$) and nearly 8 times the threshold with depolarizing noise ($R_e = 0$, $p_{\text{th}} = 1.1\%$). The latter two thresholds are slightly higher than those reported in Ref. [15], because we use the slightly more accurate MWPM decoder, instead of a weighted Union Find decoder.

Previous works using the $XZZX$ surface code to correct biased Pauli noise leverage its particular symmetry which guarantees that the pairs of error syndromes created by Z errors on the data and ancilla qubits lie in disconnected 2D planes [13,14]. This advantage vanishes in the absence of bias-preserving gates (see, for instance, Ref. [8]). The fact that we observe high thresholds with only the native gates, and relatively little additional improvement from incorporating bias-preserving CX gates for $R_e < 1$ [Fig. 1(b)], suggests that other mechanisms are responsible. This is reinforced by a separate calculation showing that the Calderbank-Shor-Steane and $XZZX$ surface codes give almost the same threshold for biased erasures with native gates at $R_e = 0.98$.

The high threshold with native gates arises from two mechanisms. First, the biased erasure model has a lower error probability than the unbiased erasure model: After returning to the qubit space, the probability of an error in the biased erasure model is $3/4$, compared to $15/16$ for the unbiased model. Second, even though Z errors can be converted into X errors in the absence of bias-preserving gates, detecting erasures after every gate allows this evolution to be tracked, lowering the entropy of noise [Fig. 1(c)] and reducing the impact of bias-preserving gates on the threshold.

Previous works on biased Pauli errors have also proposed using a thin rectangular $XZZX$ code with a smaller distance for the low-rate error [8,13], which provides an additional reduction in qubit overhead. This is not possible in the biased erasure model, without bias-preserving CX gates, because the dominant Z errors get converted to X errors. However, we see in the next section that this can be overcome using an alternate approach based on fusions.

For estimating the performance of biased erasure models in other qubit platforms that may have varying degrees of bias, and for including potential bias-degrading effects in ^{171}Yb, we parametrize a finite bias version and compute thresholds as a function of bias in Supplemental Material [44]. We find that the rate of erasures from the low-probability state (here, $|0\rangle$) must be approximately 100 times less than the high-probability state to take full advantage of the bias (similar to the case of biased Pauli noise [8,13]). While these simulations do not include errors in single-qubit gates, measurements, or idling qubits, we believe that these do not have a significant effect, because these operations are comparatively higher fidelity for neutral-atom qubits [30].

IV. HYBRID-FUSION QEC

Measurement-based error correction (MBEC) is an alternative approach to error correction based on performing local measurements on a many-body 3D entangled state called a fault-tolerant cluster state [47–51]. In the standard approach to realize a fault-tolerant cluster state, called *foliation*, one dimension of the cluster state effectively simulates time along which a planar encoded state is propagated via teleportation [52–55]. Indeed, the commonly used Raussendorf-Harrington-Goyal or Raussendorf-Bravyi-Harrington cluster state [52,53,56] teleports the standard Calderbank-Shor-Steane surface code. Similarly, the recently introduced $XZZX$ cluster state teleports the $XZZX$ surface code [57]. Given planar arrays with a finite number of qubits, a computation of length scaling exponentially with the size of the array can be performed by using as few as two of these arrays at a time [53] and teleporting the logical state back and forth between them. After a slice is measured, it is reinitialized into a cluster state.

Fusion-based error correction (FBEC) is a particular approach for MBEC in which the cluster state is grown by fusing together few-body entangled resource states. Fusions are entangling operations carried out by performing destructive two-qubit measurements of $X \otimes X$ and $Z \otimes Z$. FBEC has been widely studied for linear optical quantum computing, because fusions are the native entangling operations in that platform [25–29]. Recently, a fusion-based construction of the $XZZX$ code was proposed that can maintain the symmetry of that code under biased noise if the fusion errors are biased [29].

In this section, we introduce a *hybrid-fusion* construction of the $XZZX$ cluster state with biased erasures that combines fusion operations and deterministic entangling gates, which is optimized for the error model and capabilities of metastable ^{171}Yb qubits. After reviewing the $XZZX$ cluster state, we introduce an eight-qubit resource state (hereafter, *8-ring*) and present its construction. Next, we design a bias-preserving fusion circuit that ensures that biased erasures in the physical gates affect only the $X \otimes X$ measurements, preserving $Z \otimes Z$. Finally, we present the hybrid cluster state construction protocol that uses both fusions and direct CZ gates to entangle a collection of 8-ring resource states. The operations and resource states are designed to minimize the number of CZ gates while ensuring that biased erasures at any step maintain the two-dimensional symmetry of the $XZZX$ code. This simplifies the decoding problem, enabling higher thresholds and lower overhead [14,29], which we demonstrate using circuit-level simulations.

A. The $XZZX$ cluster state

The $XZZX$ cluster state [57] is a stabilizer state defined on a graph with an X-*type* or Z-*type* qubit at each vertex, represented by ● and ○, respectively, in Fig. 2(a). There is a stabilizer centered at each vertex. The stabilizer centered at a X-type qubit is the product of the Pauli X operator of that qubit, the Pauli Z operators of all adjacent X-type qubits, and the Pauli X operators of all the adjacent Z-type qubits. The stabilizer centered at a Z-type qubit is the product of the Pauli Z operator of that qubit and the Pauli Z operators of all adjacent X-type qubits. There is no edge between two Z-type qubits in the states considered here. Multiplying the stabilizers centered on the faces of a unit cell gives the six-body cell stabilizer, which is a product of Pauli X operators on the X-type qubits and Pauli Z operators on the Z-type qubits on the faces of the cell, as shown in Fig. 2(b). Measuring all Z-type qubits in the Z basis and all X-type qubits in the X basis teleports the $XZZX$ surface code through this cluster state.

In the $XZZX$ cluster state, a Z error on an X-type qubit or an X error on a Z-type qubit causes its neighboring cell stabilizers to flip [57]. To simultaneously perform error correction, the value of each cell stabilizer is constructed by adding the measurements outcomes of qubits around the faces of the unit cells. Importantly, Z errors on X-type qubits cause only pairs of defects, or error syndromes, that are confined to lie in disconnected 2D layers, leading to more accurate decoding of errors and higher thresholds [13,14,57]. This feature reflects the symmetry that arises within the stabilizer group of the $XZZX$ code under Z errors. To take advantage of this feature (i.e., by using a rectangular code), it is necessary to ensure that the dominant physical noise during cluster state preparation preserves this symmetry, by only introducing Z errors on X-type qubits.

This property is satisfied when using CZ gates with biased erasures to directly entangle X-type qubits. However, without a bias-preserving CX gate, it is not possible to directly entangle X- and Z-type qubits without converting the dominant Z-biased erasures to X-biased erasures and, thus, introducing unwanted X errors on the Z-type qubits. To overcome this challenge, our approach is to isolate the generation of entanglement between X- and Z-type qubits in the creation of 8-ring resource states that are postselected on the absence of erasures. These are then joined together into layers using adaptive fusion measurements which preserves the noise bias so that dominant Z-biased erasures do not introduce errors on Z-type qubits. Finally, the layers are joined to form the 3D cluster state using only CZ gates on X-type qubits.

B. The resource state

The cluster state is assembled out of a collection of 8-ring resource states. The 8-ring state is defined by the graph in Fig. 2(c) and can be prepared using the circuit in

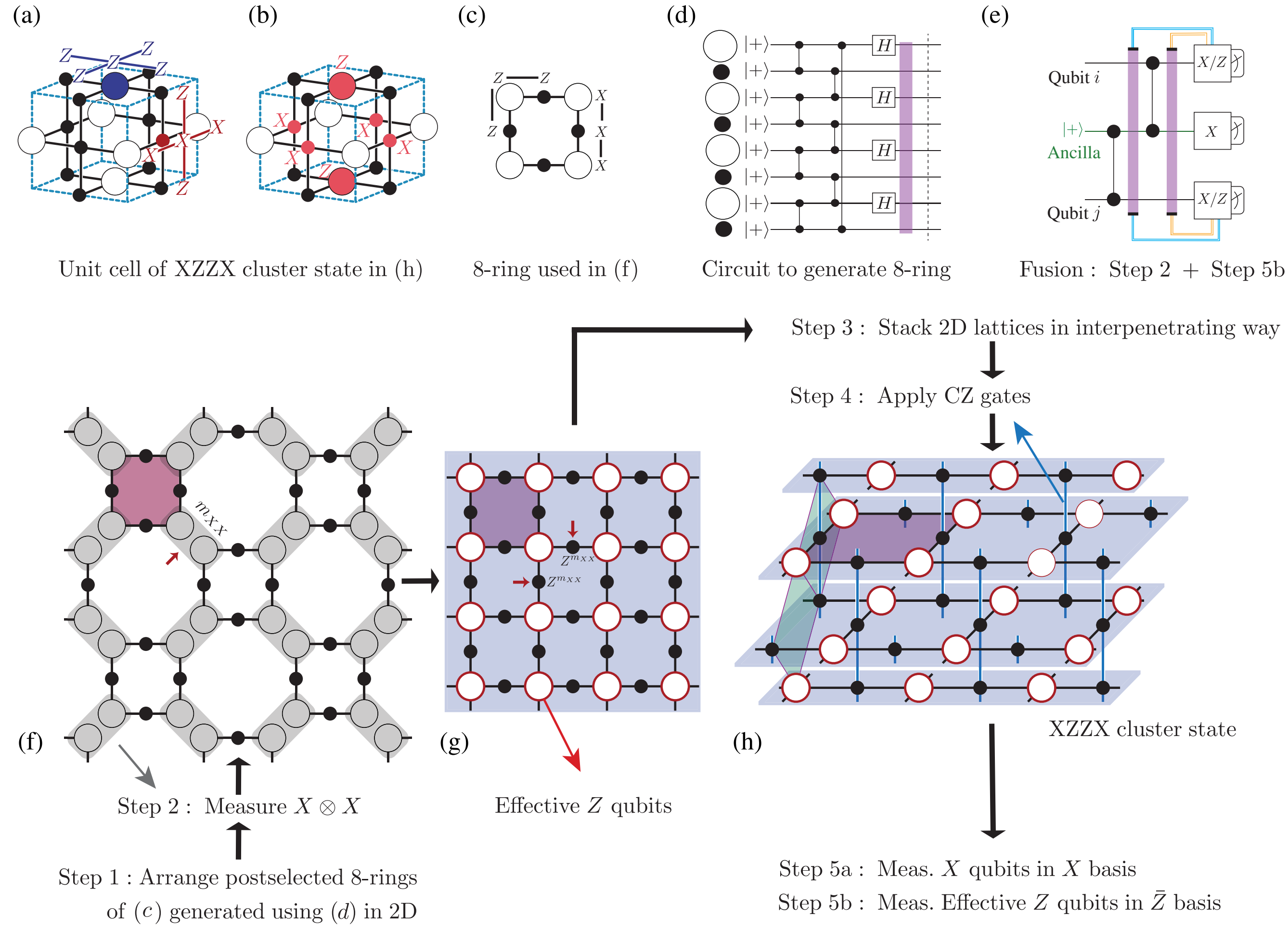

FIG. 2. (a) A unit cell of the *XZZX* cluster state, with two examples of stabilizers centered on X- (●) and Z- (○) type qubits as described in the main text. (b) The cell stabilizer obtained by multiplying the stabilizers centered at all faces of a unit cell. (c) The 8-ring resource states used to build the cluster state. (d) Circuit to generate the resource state with ^{171}Yb atoms. The state is postselected on the absence of detected erasure errors. We draw only a single erasure detection step at the end of the circuit to reflect that the precise space-time location of the errors is not needed. In practice, a fluorescence detection is performed after every gate. (e) Circuit for adaptive, bias-preserving fusion measurements with ^{171}Yb atoms. Erasure detection (via fluorescence, purple lines) is performed following each gate. If any erasures occur, the measurement basis of the fusion qubits is changed from X to Z, ensuring that the value of $Z \otimes Z$ is preserved at the expense of $X \otimes X$. (f)–(h) Extended protocol for conceptual understanding of how the cluster state error correction is realized. For reference, in (h) we highlight in green a planar array of qubits encoded in *XZZX* surface code that is being propagated in time (left to right), generating the *XZZX* cluster state. Note that the entire cluster state shown does not need to be built at once and can be realized using a small number of such planar arrays of qubits which are reused over time (see Ref. [44]).

Fig. 2(d). This circuit involves eight CZ gates between neighboring X- and Z-type qubits on a ring. Biased erasures can result in unwanted X errors on Z-type qubits. However, postselecting completed rings on the absence of erasures allows these errors to be removed while at the same time increasing the overall fidelity of the resource state. Using the notation in Sec. II, in the limit where $R_e \approx 1$ and $p_e \ll 1$, the success probability is $1 - 8p_e$, and the error probability of successful resource states is approximately $8p'_p$. Many copies of this resource state can be prepared in parallel, and the successful ones can be moved into the positions for cluster state construction, described next, using movable optical tweezers [33,58].

C. Adaptive, bias-preserving fusion measurements

A fusion measurement is a destructive two-qubit measurement of $X \otimes X$ and $Z \otimes Z$. Figure 2(e) presents an adaptive fusion measurement circuit with the property that biased erasures during two-qubit gates cause only an erasure of the $X \otimes X$ measurement outcome. In the ideal evolution without errors, the ancilla qubit measures $Z_i \otimes Z_j$ using CZ gates, followed by the single-qubit measurements $X_i \otimes I_j$ and $I_i \otimes X_j$, from which $X_i \otimes X_j$ can be computed [44].

In order to concentrate dominant errors into the $X_i \otimes X_j$ measurements and preserve the $Z_i \otimes Z_j$ information, we check for erasure errors in the two CZ gates, as shown in

Fig. 2(e), and adapt the subsequent operations based on the location of these errors. In particular, when an erasure is detected, the protocol is aborted, and each fusion qubit is measured independently in the Z basis with the measurement outcomes m_i ($= 0$ or 1) and m_j ($= 0$ or 1). The overall evolution is as if the atoms i, j are fused, with the $Z_i \otimes Z_j$ measurement outcome $= m_i \oplus m_j$, but the $X_i \otimes X_j$ measurement outcome is erased. We note that the Z measurement needs to be performed only on the fusion qubit that is not erased, because observing the erasure is equivalent to measuring the erased atom in $|1\rangle$. Therefore, the erased qubits also do not need to be replaced, unlike the approach in Sec. III and Ref. [15].

D. Constructing the *XZZX* cluster state

We now present a technique to construct the full *XZZX* cluster state using 8-rings, fusion measurements, and deterministic entangling gates. We first present the most intuitive version of the protocol [Figs. 2(f)–2(h)] and then a contracted version (Fig. 3).

1. Intuitive protocol

In step 1, copies of postselected 8-ring resource states [Figs. 2(c) and 2(d)] are arranged in a plane as shown in Fig. 2(f). In step 2, an $X \otimes X$ measurement is performed on pairs of Z-type qubits at the neighboring corners. This measurement joins the pair of measured qubits into a single effective Z-type qubit with logical Z operator $\bar{Z} = Z \otimes Z$, giving a single 2D layer of the *XZZX* cluster state shown in Fig. 2(g) [27,29]. To ensure that the postmeasurement state is the stabilizer state defined by the graph in Fig. 2(g), a Pauli Z correction is applied to the two X-type qubits adjacent to one of the measured Z-type qubits conditional on the outcome of the $X \otimes X$ measurement [29]. In practice, this correction is tracked in software.

In step 3, copies of such 2D lattices are stacked on top of each other in a staggered manner such that the X-type qubits in one layer align with those in the next, while the Z-type qubits in one layer lie on top of a face in the next layer [Fig. 2(h)]. In step 4, a CZ gate is applied between each X-type qubit in layer k and another X-type qubit at the same location in layer $k+1$ as shown in Fig. 2(h). This gives the entire 3D *XZZX* cluster state. Importantly, the CZ gates commute with each other and may be applied in any order. Here, we follow a specific order: For each X-type qubit connected to unit cells to its left and right, the CZ gate with the X-type qubit in the layer above it is performed before the CZ gate with the layer below. If an erasure is detected in the first CZ gate, the second CZ gate is omitted to avoid introducing additional errors.

Now that we have the cluster state, we measure each qubit to teleport the *XZZX* surface code through the cluster state and to reconstruct the cell stabilizers in Fig. 2(b) for error correction. This is divided into two substeps. In step 5(a), we measure each X-type qubit in X basis. In step 5(b), we measure each effective Z-type qubits in the effective $\bar{Z}$ basis, by measuring $Z \otimes Z$ on the physical Z-type qubits composing the effective qubit. This outcome is not affected by biased erasures, since the fusion circuit ensures that the $Z \otimes Z$ result is preserved.

2. Contracted protocol

We now observe that these operations can be regrouped to shorten the protocol. First, step 5(b) commutes with steps 5(a), 4, 3, and 2 and can, therefore, be performed simultaneously with step 2. Steps 5(b) and 2 together constitute a fusion measurement, which removes Z-type qubits from the cluster state entirely. This fusion measurement is implemented using the circuit in Fig. 2(e). Furthermore, the staggered layer stacking and CZ gates in steps 3 and 4, respectively, can also be performed concurrent with or before the fusion measurements, as they act on a different subset of the qubits. Thus, the sequence of operations in the shortened protocol, summarized in Fig. 3, begins by preparing several copies of postselected resource states and moving them in position to form layers stacked in a staggered manner (steps 1 and 3), which is followed by fusions [steps 2 and 5(b)] and CZ gates between layers (step 4), and finally measurement of X qubits in the X basis

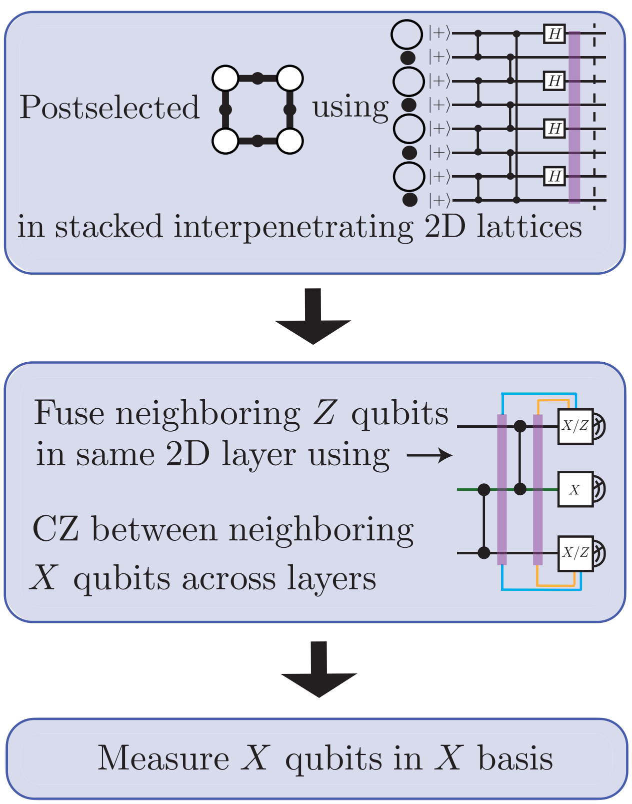

FIG. 3. Proposed shortened protocol for high-threshold hybrid-fusion QEC with the *XZZX* cluster state using fusions and CZ gates.

[step 5(a)]. Note that, in the case of a biased erasure during a fusion, we do not obtain the $X \otimes X$ measurement information, which means we cannot determine the Pauli correction on the two neighboring X-type qubits as discussed in Sec. IV C. This is effectively a random Pauli $Z \otimes Z$ error on these qubits. This correlated two-qubit error does not reduce the distance, as it is not oriented along a logical operator.

We also point out that accumulation of coherent errors, such as from the no-jump evolution, are suppressed, because every qubit is measured frequently (at most after four CZ gates). As with the circuit-based approach, additional suppression can be realized by twirling, inserting random Pauli gates before the CZ gates in resource state generation, fusion circuit, and in interlayer entangling steps.

E. Threshold results

We evaluate the performance of our hybrid-fusion architecture under the biased erasure noise model by estimating the thresholds for different R_e (Fig. 4). Our simulations account for noise in the CZ gates used in the resource state generation circuit, the fusion circuit, and the direct entanglement in step 4. Errors are decoded using the MWPM decoder and a $d \times d \times d$ cluster state, with d up to 13, which is equivalent to teleporting a $d \times d$ planar $XZZX$ code while performing d rounds of stabilizer measurements in the circuit-based approach.

For $R_e = 0.98$, we obtain a threshold of 10.3%, higher than that achieved with the circuit-based approach with or without bias-preserving CX gates. In the other extreme of $R_e = 0$ when all source of noise is depolarizing Pauli noise, we obtain a threshold of 1%, similar to the threshold with circuit-based error correction at the same value of R_e.

In the limit $R_e = 1$, we achieve a threshold of 14.7%. This threshold can also be determined from the bond-percolation threshold of the union-jack lattice and is expected to be approximately 17.7% [44]. The observed threshold in Fig. 4 is smaller than this because of finite size effects that are more prominent in the extreme case of $R_e = 1$ when the decoding graph is 2D. To confirm, we use a fast erasure decoder [59] to simulate extremely large lattices ($d \times d \times 5$ up to $d = 61$) and recover the threshold predicted by percolation theory in this limit. Since the erasure decoder and MWPM decoder achieve the same accuracy for erasure errors, we believe that we should achieve the same thresholds for both decoders at $R_e = 1$, but simulating such large lattices with MWPM is computationally prohibitive.

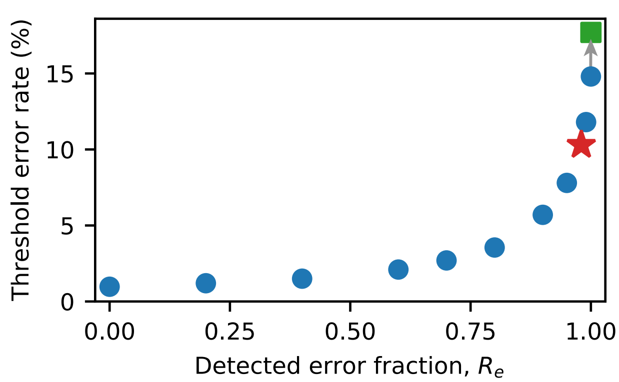

FIG. 4. Threshold error rates for the hybrid-fusion architecture as a function of erasure fraction, R_e. The star denotes $R_e = 98\%$, while the green square marks the percolation threshold corresponding to the decoding graph for $R_e = 1$ (see the text).

F. Comparison to other approaches to generating a cluster state

The benefit of the hybrid-fusion approach can be understood by comparison to alternative cluster state constructions. Compared to directly entangling all the qubits in the cluster state, our hybrid-fusion approach results in the same number of biased erasure errors on the final cluster state but ensures that the error syndromes lie in disconnected 2D layers. However, the number of CZ gates, and, thus, the rough Pauli error rate on the final cluster state, is increased by a factor of 4/3. Therefore, our approach should outperform direct entanglement except when R_e is very small and Pauli errors are more important to correct than biased erasures.

On the other hand, we can compare to an all-fusion strategy like the 6-ring construction of Ref. [29]. Our strategy again has the same number of biased erasure errors on the final cluster state but uses 2/3 the number of CZ gates. Therefore, our approach outperforms the all-fusion construction except when $R_e \gtrsim 0.99$, where the higher percolation threshold of the decoding graph in the all-fusion approach gives a slight advantage.

V. DISCUSSION

We now make several comparisons between the presented circuit-based and hybrid-fusion approaches. Our hybrid-fusion protocol can be viewed as implementing QEC on a state encoded in a planar $XZZX$ code as it is being teleported to another planar array of qubits. This is an alternative to using repeated rounds of quantum nondemolition stabilizer measurements as in conventional circuit-based error correction but still allows transversal one- and two-qubit logical gate operations available for the planar surface code. In Supplemental Material, we explicitly show how our hybrid-fusion protocol can be implemented with just a few planar arrays of qubits, starting and stopping with a 2D encoded $XZZX$ surface code [44]. We note that neutral atoms are ideally suited to the high degree of connectivity required to implement hybrid fusion: Dynamic rearrangement of qubits is already used to postselect filled tweezer sites [60,61], and coherent qubit transport has also been demonstrated [33,58].

The hybrid-fusion approach has other advantages beyond the higher threshold, which we outline here but do not quantitatively analyze. As discussed, our construction preserves the system symmetry of the $XZZX$ code under biased noise by ensuring that the high-probability Z erasures run along layers in Fig. 2(h). Thus, the same logical error rate can be achieved with fewer layers when R_e is large and the erasure are highly biased. This amounts to using a thin, rectangular $XZZX$ surface code, which becomes a repetition code when $R_e = 1$ and the erasures are infinitely biased [13]. This allows for reduced overhead compared to the circuit-based approach, which requires a square $XZZX$ code in the absence of bias-preserving gates. This property is summarized for each QEC architecture in Table I.

Second, the teleportation process converts lost atoms into Pauli errors, ensuring a finite threshold against loss errors or undetected erasures without additional leakage reduction units [62–66]. We leave an analysis of the threshold for a given loss rate to future work.

Finally, hybrid-fusion QEC relaxes the requirements for erasure detection and subsequent atom replacement. In the circuit-approach proposed in Ref. [15] and considered in Sec. III, the space-time location of each erasure error in the circuit must be resolved, and the affected qubits must be replaced or reinitialized as the computation proceeds. In the hybrid-fusion approach, this requirement is relaxed, in a way that is slightly different for the three steps involving two-qubit gates. For resource state preparation (step 1 of the protocol in Sec. IV D), it is necessary only to determine if an erasure occurred at some point during the 8-ring preparation, and if it did, the entire state is discarded. Therefore, there is no need to replace affected qubits, and the necessary spatiotemporal resolution of the erasure detection is significantly coarser. During the fusion operations [steps 2 and 5(b)], erasures must be detected immediately as the measurement basis is conditioned on this outcome, but the affected atoms do not need to be replaced. Finally, in the layer-joining CZ gates (step 4), atom replacement is not necessary, as the atoms are immediately measured. In summary, we find that conditionally replacing atoms at precise space-time locations is never required (as indicated in Table I), and in some cases erasures can be detected with coarser resolution. These may give rise to considerable experimental simplifications.

VI. CONCLUSION

In summary, we have introduced a new noise model, biased erasure, that is physically motivated by metastable ^{171}Yb qubits but may also be engineered in other qubit platforms. We have studied two realistic QEC architectures under this noise model. The first is a circuit-based approach, where the improvement with the biased erasure model arises from the reduced entropy of this noise model, enabling more effective decoding. We obtain a threshold of 8.2% for the predicted metastable ^{171}Yb erasure fraction. The second is a hybrid-fusion approach with a systematic code construction that gives rise to system symmetries under the biased erasure model. In this approach, we obtain a threshold of 10.3% for the metastable ^{171}Yb noise model. Compared to circuit-based syndrome extraction, this approach has the additional benefits of potentially enabling rectangular surface codes with lower overhead (in the limit of a large erasure fraction), robustness against atom loss, and simplified requirements for detecting and handling erasure errors in real time.

While in this work we focus on thresholds for quantum memory, we can apply Clifford gates using standard techniques such as braiding [52,53], lattice surgery [67,68], or other code deformations [69]. These can be straightforwardly adapted to our hybrid-fusion approach by modifying the large-scale shape of our cluster state but using the same underlying resource states and without affecting the thresholds [27,55,70]. In addition, we can consider entangling logical surface-code qubits via transversal CNOT gates as proposed in [71], thanks to the movability of neutral-atom qubits [33,58]; this may allow for significant overhead reduction compared to lattice surgery. To apply non-Clifford gates, we can inject noisy magic states and perform magic-state distillation [72]. We note that the erasure errors during magic-state injection may be removed by postselection, so that injected magic states are susceptible only to low-probability Pauli errors. This will aid in reducing the overhead cost of magic-state distillation.

There are several opportunities for further simplification and optimization of the hybrid-fusion approach for scalable fault-tolerant quantum computing. First, the threshold for hybrid-fusion QEC may be further improved by postselecting on larger resource states [28]. This will decrease the rate of successfully generating the resource states, but it is still an experimentally viable route with deterministic, high-fidelity gates. For example, given a gate with 99.9% CZ fidelity, resource state chunks involving 100 CZ gates could be postselected with 90% success probability. Second, we can explore error correction beyond the planar surface code, as the hybrid-fusion approach naturally allows conversion of the planar surface code to a 3D surface code with transversal non-Clifford gates [73–77], which may lead to significant overhead reduction compared to alternative protocols for non-Clifford gates that rely on magic-state distillation.

Finally, our hybrid-fusion-based construction provided a means to preserve the symmetries of the $XZZX$ code without bias-preserving CX gates by using postselection and short-depth circuits. This approach also provides a path for high-threshold QEC with biased-Pauli-noise qubits without bias-preserving CX gates, which is an open challenge so far.

ACKNOWLEDGMENTS

We acknowledge Steve Flammia for pointing out the importance of lowered noise entropy. We are also grateful to Shimon Kolkowitz, Steve Girvin, Shilin Huang, Shuo Ma, and Yue Wu for helpful discussions. This work was supported by the National Science Foundation (QLCI Grant No. OMA-2120757). J. D. T. acknowledges additional support from ARO PECASE (W911NF-18-10215), ONR (N00014-20-1-2426), DARPA ONISQ (W911NF-20-10021), and the Sloan Foundation.

[1] Peter W. Shor, *Scheme for reducing decoherence in quantum computer memory*, Phys. Rev. A **52**, R2493 (1995).
[2] P. W. Shor, *Fault-tolerant quantum computation*, in *Proceedings of the 37th Conference on Foundations of Computer Science, Burlington, VT, USA* (IEEE, 1996), pp. 56–65, https://ieeexplore.ieee.org/document/548464.
[3] A. R. Calderbank and Peter W. Shor, *Good quantum error-correcting codes exist*, Phys. Rev. A **54**, 1098 (1996).
[4] Dorit Aharonov and Michael Ben-Or, *Fault-tolerant quantum computation with constant error*, in *Proceedings of the Twenty-Ninth Annual ACM Symposium on Theory of Computing* (Association for Computing Machinery, New York, 1997), pp. 176–188.
[5] Emanuel Knill, Raymond Laflamme, and Wojciech H Zurek, *Resilient quantum computation*, Science **279**, 342 (1998).
[6] Daniel Gottesman, *Theory of fault-tolerant quantum computation*, Phys. Rev. A **57**, 127 (1998).
[7] John Preskill, *Reliable quantum computers*, Proc. R. Soc. A **454**, 385 (1998).
[8] Andrew S. Darmawan, Benjamin J. Brown, Arne L. Grimsmo, David K. Tuckett, and Shruti Puri, *Practical quantum error correction with the XZZX code and Kerr-cat qubits*, PRX Quantum **2**, 030345 (2021).
[9] Jérémie Guillaud and Mazyar Mirrahimi, *Repetition cat qubits for fault-tolerant quantum computation*, Phys. Rev. X **9**, 041053 (2019).
[10] Christopher Chamberland, Kyungjoo Noh, Patricio Arrangoiz-Arriola, Earl T. Campbell, Connor T. Hann, Joseph Iverson, Harald Putterman, Thomas C. Bohdanowicz, Steven T. Flammia, Andrew Keller *et al.*, *Building a fault-tolerant quantum computer using concatenated cat codes*, PRX Quantum **3**, 010329 (2022).
[11] Iris Cong, Harry Levine, Alexander Keesling, Dolev Bluvstein, Sheng-Tao Wang, and Mikhail D. Lukin, *Hardware-efficient, fault-tolerant quantum computation with Rydberg atoms*, Phys. Rev. X **12**, 021049 (2022).
[12] Shruti Puri, Lucas St-Jean, Jonathan A. Gross, Alexander Grimm, Nicholas E. Frattini, Pavithran S. Iyer, Anirudh Krishna, Steven Touzard, Liang Jiang, Alexandre Blais *et al.*, *Bias-preserving gates with stabilized cat qubits*, Sci. Adv. **6**, 5901 (2020).
[13] J. Pablo Bonilla Ataides, David K. Tuckett, Stephen D. Bartlett, Steven T. Flammia, and Benjamin J. Brown, *The XZZX surface code*, Nat. Commun. **12**, 1 (2021).
[14] Benjamin J. Brown, *Conservation laws and quantum error correction: Towards a generalised matching decoder*, arXiv:2207.06428.
[15] Yue Wu, Shimon Kolkowitz, Shruti Puri, and Jeff D. Thompson, *Erasure conversion for fault-tolerant quantum computing in alkaline earth Rydberg atom arrays*, Nat. Commun. **13**, 4657 (2022).
[16] Mingyu Kang, Wesley C. Campbell, and Kenneth R. Brown, *Quantum error correction with metastable states of trapped ions using erasure conversion*, PRX Quantum **4**, 020358 (2023).
[17] Aleksander Kubica, Arbel Haim, Yotam Vaknin, Fernando Brandão, and Alex Retzker, *Erasure qubits: Overcoming the T_1 limit in superconducting circuits*, arXiv:2208.05461.
[18] James D. Teoh, Patrick Winkel, Harshvardhan K. Babla, Benjamin J. Chapman, Jahan Claes, Stijn J. de Graaf, John W. O. Garmon, William D. Kalfus, Yao Lu, Aniket Maiti *et al.*, *Dual-rail encoding with superconducting cavities*, arXiv:2212.12077.
[19] Thomas M. Stace, Sean D. Barrett, and Andrew C. Doherty, *Thresholds for topological codes in the presence of loss*, Phys. Rev. Lett. **102**, 200501 (2009).
[20] Sean D. Barrett and Thomas M. Stace, *Fault tolerant quantum computation with very high threshold for loss errors*, Phys. Rev. Lett. **105**, 200502 (2010).
[21] Adam C. Whiteside and Austin G. Fowler, *Upper bound for loss in practical topological-cluster-state quantum computing*, Phys. Rev. A **90**, 052316 (2014).
[22] Wesley C. Campbell, *Certified quantum gates*, Phys. Rev. A **102**, 022426 (2020).
[23] M. Grassl, Th. Beth, and T. Pellizzari, *Codes for the quantum erasure channel*, Phys. Rev. A **56**, 33 (1997).
[24] Charles H. Bennett, David P. DiVincenzo, and John A. Smolin, *Capacities of quantum erasure channels*, Phys. Rev. Lett. **78**, 3217 (1997).
[25] Daniel E. Browne and Terry Rudolph, *Resource-efficient linear optical quantum computation*, Phys. Rev. Lett. **95**, 010501 (2005).
[26] Ying Li, Peter C. Humphreys, Gabriel J. Mendoza, and Simon C. Benjamin, *Resource costs for fault-tolerant linear optical quantum computing*, Phys. Rev. X **5**, 041007 (2015).
[27] Sara Bartolucci, Patrick Birchall, Hector Bombin, Hugo Cable, Chris Dawson, Mercedes Gimeno-Segovia, Eric Johnston, Konrad Kieling, Naomi Nickerson, Mihir Pant *et al.*, *Fusion-based quantum computation*, Nat. Commun. **14**, 912 (2023).
[28] Stefano Paesani and Benjamin J. Brown, *High-threshold quantum computing by fusing one-dimensional cluster states*, arXiv:2212.06775.
[29] Kaavya Sahay, Jahan Claes, and Shruti Puri, *Tailoring fusion-based error correction for high thresholds to biased fusion failures*, arXiv:2301.00019.
[30] Shuo Ma, Genyue Liu, Pai Peng, Bichen Zhang, Sven Jandura, Jahan Claes, Alex P. Burgers, Guido Pupillo, Shruti Puri, and Jeff D. Thompson, *High-fidelity gates with mid-circuit erasure conversion in a metastable neutral atom qubit*, arXiv:2305.05493.

[31] Yao Lu, Aniket Maiti, John W. O. Garmon, Suhas Ganjam, Yaxing Zhang, Jahan Claes, Luigi Frunzio, S. M. Girvin, and Robert J. Schoelkopf, *A high-fidelity microwave beamsplitter with a parity-protected converter*, arXiv:2303.00959.

[32] Kevin S. Chou *et al.*, *Demonstrating a superconducting dual-rail cavity qubit with erasure-detected logical measurements*, arXiv:2307.03169.

[33] Dolev Bluvstein, Harry Levine, Giulia Semeghini, Tout T. Wang, Sepehr Ebadi, Marcin Kalinowski, Alexander Keesling, Nishad Maskara, Hannes Pichler, Markus Greiner, Vladan Vuletić, and Mikhail D. Lukin, *A quantum processor based on coherent transport of entangled atom arrays*, Nature (London) **604**, 451 (2022).

[34] T. M. Graham *et al.*, *Multi-qubit entanglement and algorithms on a neutral-atom quantum computer*, Nature (London) **604**, 457 (2022).

[35] Shuo Ma, Alex P. Burgers, Genyue Liu, Jack Wilson, Bichen Zhang, and Jeff D. Thompson, *Universal gate operations on nuclear spin qubits in an optical tweezer array of* ^{171}Yb *Atoms*, Phys. Rev. X **12**, 021028 (2022).

[36] Nathan Schine, Aaron W. Young, William J. Eckner, Michael J. Martin, and Adam M. Kaufman, *Long-lived Bell states in an array of optical clock qubits*, Nat. Phys. **18**, 1067 (2022).

[37] Mark Saffman, T. G. Walker, and Klaus Mølmer, *Quantum information with Rydberg atoms*, Rev. Mod. Phys. **82**, 2313 (2010).

[38] Alec Jenkins, Joanna W. Lis, Aruku Senoo, William F. McGrew, and Adam M. Kaufman, *Ytterbium nuclear-spin qubits in an optical tweezer array*, Phys. Rev. X **12**, 021027 (2022).

[39] Sven Jandura, Jeff D. Thompson, and Guido Pupillo, *Optimizing Rydberg gates for logical qubit performance*, PRX Quantum **4**, 020336 (2023).

[40] Charles Fromonteil, Dolev Bluvstein, and Hannes Pichler, *Protocols for Rydberg entangling gates featuring robustness against quasi-static errors*, PRX Quantum **4**, 020335 (2023).

[41] Emanuel Knill, *Quantum computing with realistically noisy devices*, Nature (London) **434**, 39 (2005).

[42] Lorenza Viola and Emanuel Knill, *Random decoupling schemes for quantum dynamical control and error suppression*, Phys. Rev. Lett. **94**, 060502 (2005).

[43] Joel J. Wallman and Joseph Emerson, *Noise tailoring for scalable quantum computation via randomized compiling*, Phys. Rev. A **94**, 052325 (2016).

[44] See Supplemental Material at http://link.aps.org/supplemental/10.1103/PhysRevX.13.041013 for details of the biased-erasure error channel and an extended discussion on the circuit-based and hybrid-fusion implementations.

[45] Craig Gidney, *STIM: A fast stabilizer circuit simulator*, Quantum **5**, 497 (2021).

[46] Oscar Higgott, *PyMatching: A PYTHON package for decoding quantum codes with minimum-weight perfect matching*, ACM Trans. Quantum Comput. **3**, 1 (2022).

[47] Hans J. Briegel and Robert Raussendorf, *Persistent entanglement in arrays of interacting particles*, Phys. Rev. Lett. **86**, 910 (2001).

[48] Robert Raussendorf and Hans J. Briegel, *A one-way quantum computer*, Phys. Rev. Lett. **86**, 5188 (2001).

[49] Robert Raussendorf, Daniel E. Browne, and Hans J. Briegel, *The one-way quantum computer—a non-network model of quantum computation*, J. Mod. Opt. **49**, 1299 (2002).

[50] Robert Raussendorf, Daniel E. Browne, and Hans J. Briegel, *Measurement-based quantum computation on cluster states*, Phys. Rev. A **68**, 022312 (2003).

[51] Hans J. Briegel, David E. Browne, Wolfgang Dür, Robert Raussendorf, and Maarten Van den Nest, *Measurement-based quantum computation*, Nat. Phys. **5**, 19 (2009).

[52] Robert Raussendorf, Jim Harrington, and Kovid Goyal, *A fault-tolerant one-way quantum computer*, Ann. Phys. (Amsterdam) **321**, 2242 (2006).

[53] Robert Raussendorf and Jim Harrington, *Fault-tolerant quantum computation with high threshold in two dimensions*, Phys. Rev. Lett. **98**, 190504 (2007).

[54] A. Bolt, G. Duclos-Cianci, D. Poulin, and T. M. Stace, *Foliated quantum error-correcting codes*, Phys. Rev. Lett. **117**, 070501 (2016).

[55] Benjamin J. Brown and Sam Roberts, *Universal fault-tolerant measurement-based quantum computation*, Phys. Rev. Res. **2**, 033305 (2020).

[56] Robert Raussendorf, Sergey Bravyi, and Jim Harrington, *Long-range quantum entanglement in noisy cluster states*, Phys. Rev. A **71**, 062313 (2005).

[57] Jahan Claes, J. Eli Bourassa, and Shruti Puri, *Tailored cluster states with high threshold under biased noise*, npj Quantum Inf. **9**, 9 (2023).

[58] Jérôme Beugnon, Charles Tuchendler, Harold Marion, Alpha Gaëtan, Yevhen Miroshnychenko, Yvan R. P. Sortais, Andrew M. Lance, Matthew P. A. Jones, Gaétan Messin, Antoine Browaeys, and Philippe Grangier, *Two-dimensional transport and transfer of a single atomic qubit in optical tweezers*, Nat. Phys. **3**, 696 (2007).

[59] Nicolas Delfosse and Gilles Zémor, *Linear-time maximum likelihood decoding of surface codes over the quantum erasure channel*, Phys. Rev. Res. **2**, 033042 (2020).

[60] Manuel Endres, Hannes Bernien, Alexander Keesling, Harry Levine, Eric R. Anschuetz, Alexandre Krajenbrink, Crystal Senko, Vladan Vuletic, Markus Greiner, and Mikhail D. Lukin, *Atom-by-atom assembly of defect-free one-dimensional cold atom arrays*, Science **354**, 1024 (2016).

[61] Daniel Barredo, Sylvain de Léséluc, V. Lienhard, T. Lahaye, and A. Browaeys, *An atom-by-atom assembler of defect-free arbitrary two-dimensional atomic arrays*, Science **354**, 1021 (2016).

[62] Emanuel Knill, *Scalable quantum computing in the presence of large detected-error rates*, Phys. Rev. A **71**, 042322 (2005).

[63] Panos Aliferis and Barbara M. Terhal, *Fault-tolerant quantum computation for local leakage faults*, Quantum Inf. Comput. **7**, 139 (2007).

[64] Austin G. Fowler, *Coping with qubit leakage in topological codes*, Phys. Rev. A **88**, 042308 (2013).

[65] Joydip Ghosh and Austin G. Fowler, *Leakage-resilient approach to fault-tolerant quantum computing with superconducting elements*, Phys. Rev. A **91**, 020302(R) (2015).

[66] Martin Suchara, Andrew W. Cross, and Jay M. Gambetta, *Leakage suppression in the Toric code*, in *Proceedings of the 2015 IEEE International Symposium on Information Theory (ISIT)* (IEEE, New York, 2015), pp. 1119–1123.

[67] Clare Horsman, Austin G. Fowler, Simon Devitt, and Rodney Van Meter, *Surface code quantum computing by lattice surgery*, New J. Phys. **14**, 123011 (2012).

[68] Daniel Litinski, *A game of surface codes: large-scale quantum computing with lattice surgery*, Quantum **3**, 128 (2019).

[69] Benjamin J. Brown, Katharina Laubscher, Markus S. Kesselring, and James R. Wootton, *Poking holes and cutting corners to achieve Clifford gates with the surface code*, Phys. Rev. X **7**, 021029 (2017).

[70] Daniel Herr, Alexandru Paler, Simon J. Devitt, and Franco Nori, *Lattice surgery on the Raussendorf lattice*, Quantum Sci. Technol. **3**, 035011 (2018).

[71] Eric Dennis, Alexei Kitaev, Andrew Landahl, and John Preskill, *Topological quantum memory*, J. Math. Phys. (N.Y.) **43**, 4452 (2002).

[72] Sergey Bravyi and Alexei Kitaev, *Universal quantum computation with ideal Clifford gates and noisy Ancillas*, Phys. Rev. A **71**, 022316 (2005).

[73] Hector Bombin, *2D quantum computation with 3D topological codes*, arXiv:1810.09571.

[74] Michael Vasmer and Dan E. Browne, *Three-dimensional surface codes: Transversal gates and fault-tolerant architectures*, Phys. Rev. A **100**, 012312 (2019).

[75] Benjamin J. Brown, *A fault-tolerant non-Clifford gate for the surface code in two dimensions*, Sci. Adv. **6**, aay4929 (2020).

[76] T. R. Scruby, D. E. Browne, P. Webster, and M. Vasmer, *Numerical implementation of just-in-time decoding in novel lattice slices through the three-dimensional surface Code*, Quantum **6**, 721 (2022).

[77] Zhenyu Cai, Adam Siegel, and Simon Benjamin, *Looped pipelines enabling effective 3D qubit lattices in a strictly 2D device*, PRX Quantum **4**, 020345 (2023).